Spectroscopic sensing with silicon nitride photonic integrated circuits

(invited paper)

S. Clemmen[1,2], A. Raza[1,2], A. Dhakal[1,2,5*], F. Peyskens[1,2], A. Subramanian[1,2], P. Van Dorpe[4], P. Wuytens[1,2,3], H. Zhao[1,2], E. Ryckeboer[1,2], S. Severi[4], N. Le Thomas[1,2], R. Baets[1,2],

1. Photonics Research Group, INTEC Department, Ghent University - imec, Belgium
2. Center for Nano- and Biophotonics, Ghent University, Belgium
3. Department of Molecular Biotechnology, Ghent University, Belgium
4. imec, Kapeldreef 75, 3001 Heverlee, Belgium
5. *current address: Phutung Research Institute, Balaju, Kathmandu, Nepal

1. INTRODUCTION

Raman spectroscopy is a mature technology capable of identifying the chemical composition of nearly any sample based on the resonance frequencies of individual molecular bonds. Applications of Raman spectroscopy are extremely broad ranging from biology, chemistry, pharmaceutics, art preservation, or various monitoring [1].
In its most prevalent form, a Raman spectrometer consists of a laser, a focusing objective - often within a microscope -, a spectrometer, and a camera. As Raman spectroscopy relies on the very weak inelastic scattering of light onto matter, the laser has to deliver a relatively high power (10s mW) and the detector needs to be very sensitive and noise free. The detection is currently the bottleneck that prevents Raman spectroscopy to be even more broadly used. The detection is indeed expensive both in term of time and equipment cost. Therefore, many solutions have been investigated to relax the requirement for a state of the art detector by boosting the Raman response. Stimulated Raman spectroscopy[2] allows using more noisy detectors but at the cost of an extra more complex laser. Surface enhanced Raman spectroscopy (SERS) is another enhancement technique that takes advantage of plasmonic enhancement to increase locally the Raman response of an analyte [3]. Various SERS substrates have been developed and are commercially available. Those show a large increase in Raman signals but often at the expense of spectral reproducibility. SERS substrates based on patterned plasmonic antenna suffer much less from reproducibility issues [4] but are usually much more demanding in terms of fabrication which requires nm-level resolution and are therefore not cheap. Raman signals can also be enhanced via an interaction with more molecules thanks to a waveguiding structure such as a hollow core fiber [5] or a photonic waveguide [6,7, 8, 9]. A hollow core fiber can indeed provide orders of magnitude improvement but loading the fiber with the liquid analyte in a micron scale core over a long length is neither trivial nor fast. Planar slab waveguides have also shown great Raman enhancement but remain limited by diffraction. More recently, photonic rib waveguides have shown great Raman enhancement [10] over lengths only limited by the propagation loss of the waveguide. Moreover, photonic circuits have the added benefit of allowing compact and cheap spectral functionalities such as arrayed waveguide gratings (AWG), stationary Fourier spectrometer [11], or ring filters [12]. Integrating together a Raman sensor and a spectrometer on a single chip with a simple CMOS camera in a compact and cheap package is therefore very appealing. Here, we are reviewing the recent progress necessary to reach such integration.

2. STRIP-WAVEGUIDE-BASED ON-CHIP RAMAN SPECTROSCOPY

Among the multiple platforms for integrated photonics circuits, silicon nitride has the benefit of being compatible with CMOS fabrication, being transparent to wavelengths that are suitable for Raman spectroscopy and can be engineered to provide a low level of fluorescence [13]. Our first demonstration of on-chip Raman spectroscopy [10] made use of a silicon nitride rib waveguide engineered to maximize the excitation and collection of the Raman signal as depicted in figure 1a. The geometry of the rib waveguide was indeed chosen as a tradeoff

(a)

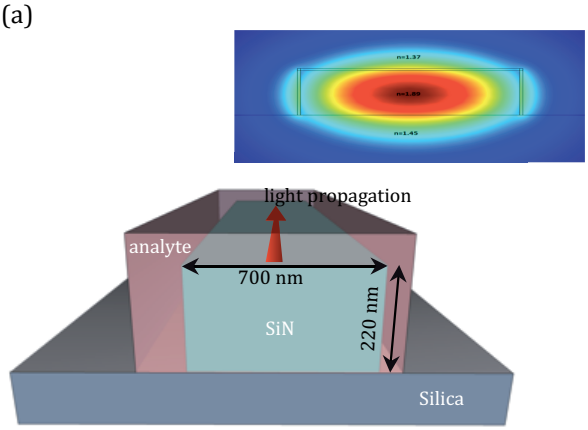

(b)

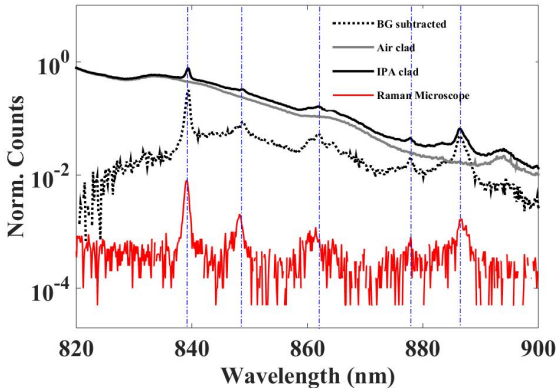

Figure1. (a) Cross-section of a rib waveguide interfacing light with an analyte via evanescent coupling. Refractive indices are n_{sin} = 1.89, n_{silica} = 1.45 and for isopropanol (IPA) taken as an analyte n_{ipa} = 1.37. Inset: modal profile (warm colors represent strong field). (b) Raman spectra measured in transmission from a waveguide covered with IPA (black line), covered with air (grey line) and resulting IPA spectra after background subtraction (dotted line). The Raman spectrum (red line) taken using a conventional confocal Raman microscope in the same conditions and the vertical dashed lines highlight the characteristic spectral lines of IPA.

between a large evanescent field capable of optically exciting as many molecules from the analyte as possible and an effective index contrast sufficient to allow efficient collection of the scattered light into the waveguide mode [14]. Formally, we can define a parameter called the *integrated luminosity* that is the excitation efficiency of a particle located at a position *r* by the guided mode and the subsequent collection of the light in the same optical mode.

$$\Lambda_{wg}(\mathbf{r}) = \frac{P_{wg}(\mathbf{r})}{\sigma P_{pump}} \qquad \text{(eq. 1)}$$

This parameter is simply the ratio of the Raman-scattered optical power collected P_{wg} to incident pump power P_{pump} for a unit scattering cross section σ. By integrating this parameter over the volume of interest, we can have an estimate of the total *Raman conversion efficiency* η, that is the ratio between the accumulated Raman generated signal and the incident optical power. In the case of a rib waveguide, the volume of interest is the one probed by the evanescent tail of the guided mode along the length of the waveguide. For a liquid analyte acting as the optical top cladding of the waveguide (see figure 1a), the density ρ of the Raman medium is uniform and there is a symmetry along the length of propagation *l* so that the integral becomes

$$\eta = \frac{P_{tot}}{P_{pump}} = \sigma \rho \, l \underbrace{\iint_S \Lambda_{wg}(\mathbf{r}) \mathrm{d}\mathbf{r}}_{\eta_0} \qquad \text{(eq. 2)}$$

This conversion efficiency thus depends on the exact field distribution in the vicinity of the waveguide and therefore requires numerical simulation (for more details see [10, 14]) accounting for the shape of the waveguide, its refractive index, the refractive index of the optical claddings, the polarization, and the wavelengths involved. Experimentally, the optimal design is further constrained by the given thickness of the nitride-guiding layer, set to 220 nm in this work. We also set the exciting wavelength at 785 nm so that the entire Raman spectrum lies in the so-called "biological spectral window" between 700 and 1000 nm. We take isopropanol (IPA) as a reference analyte having a refractive index of 1.37. With all those constraints, the optimal width of the waveguide is 600 nm for TE-polarized light. There is however very little variation in overall excitation/collection efficiency η for widths varying between 500 and 700nm so that experimentally 700 nm is preferred as it allows for smaller bending radii and therefore for sensors with a smaller footprint.

(a) (b)

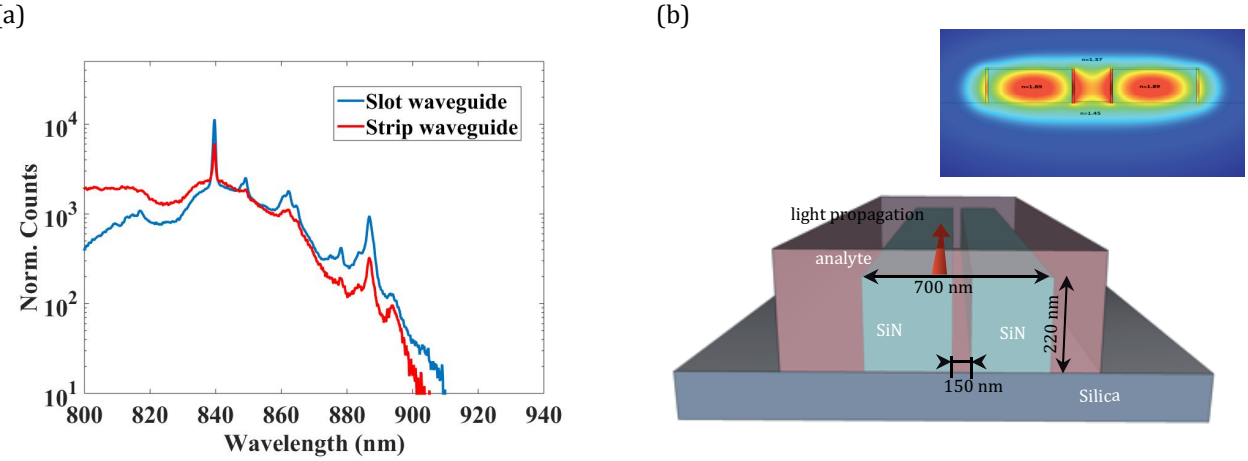

Figure2 (a) Raman spectra of IPA measured using a rib waveguide (red) and a slot-waveguide (blue) after background subtraction using water as the optical cladding material. In both case, the excitation power is set to 50 mW and the collection time is 7s. (b) Cross-section of a slot waveguide covered with IPA. Inset: modal profile (warm colors represent strong field).

The Raman spectra from such a structure is presented in figure 1b. The bold red curve corresponds to the Raman spectrum obtained in transmission from the SiN waveguide covered by a droplet of IPA and it is compared to the Raman spectra of IPA taken under identical condition (same excitation parameter, same coupling efficiency into the spectrometer) with a Raman microscope. The graph shows clearly the large improvement (2 orders of magnitude) of the IPA Raman peaks but it also shows a broadband background that is due to the waveguide itself. This background can be measured independently from a waveguide covered with air. Its origin remains subject to debate but it behaves in every aspect as Raman scattering: it scales linearly with the power and its spectrum is independent of the excitation wavelength (unlike fluorescence). Background subtraction can therefore be performed to retrieve a clean spectrum (see dotted curve in figure 1b). Unfortunately, the subtraction is not perfect because the field profile with and without IPA is not the same. Indeed, the presence of IPA affects the confinement in the waveguide. In practice however, Raman spectroscopy is often used to measure change in concentration: the concentration of IPA in solution for instance. In that case, the background subtraction procedure can be made more accurate as there is minimal change in refractive index between water (1.33) and pure IPA (1.37). The red curve in figure 2a shows the results of background subtraction when the background is measured in presence of water rather than air. Even better background subtraction is possible [15] for the specific case of waveguide-based Raman spectroscopy.

3. SLOT-WAVEGUIDE-BASED ON-CHIP RAMAN SPECTROSCOPY

While the background can be subtracted in most conditions, its presence is certainly an important limitation because the fluctuations on this extra photon flux (due to shot noise) require more averaging for a proper subtraction. Strategies have thus been investigated to reduce proportionally this background against the useful Raman spectrum. A solution consists in using a waveguide geometry capable of confining the light more efficiently into the analyte. A slot-waveguide is such a geometry (see fig 2.b). The TE-mode in such a geometry is mostly confined in the slot of the photonic structure, increasing therefore the Raman response due to the analyte and decreasing the background due to nitride. Here, we rely on a slot-waveguide having an identical width as the strip waveguide (700 nm) and a slot width of 150 nm. This geometry is quite far from an optimal design but is compatible with 193-nm photolithography in a CMOS fab. A better geometry would require a thicker SiN core and a narrower slot width. Figure 3a, shows the direct comparison between the Raman signal of IPA collected from a slot-waveguide and the one originating from a rib waveguide, both are 1.6 cm-long. In both cases the background has been subtracted thus leaving only its associated noise visible at small frequencies. The slot waveguides exhibit an improvement in signal to noise ratio by a factor of 5.

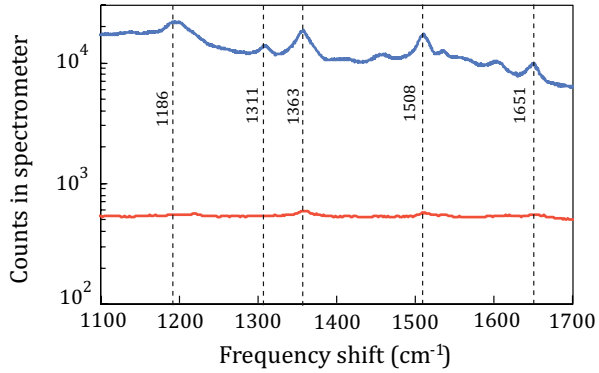

Fig 3. Comparison between confocal microscope based Raman spectroscopy (red) and slot-waveguide based Raman spectroscopy (blue) for the case of a monolayer of Rhodamine 6G. The blue curve is taken 10 times faster and with 40 times less optical power.

Apart from dilute solutions, another challenging analyte to probe with a Raman microscope is a single monolayer. Thin layers are of interest in many contexts such as biology as selective binding can occur at a dedicated functionalized layers, surface chemistry that may be relevant at electrodes, dynamics at the surface of microorganisms or cells, studying the crystalline phase of very thin layers deposited via atomic layer deposition etc. For the specific case of a monolayer, a typical Raman microscope also suffers from background issues as the monolayer has to be deposited on a substrate so that the fraction of this substrate in the confocal volume is typically very large. Indeed, the thickness of a monolayer can be on the order of 1 nm while the Rayleigh range in a confocal Raman microscope is typically on the order of 1 µm. The SNR is therefore usually quite bad in that case. In the case of a guided structure, the relative complexity of the mode profiles makes the situation a bit more complex: the field also sees a large fraction of "substrate" (guiding) material and a relatively small amount of the material under investigation but a great advantage is that this material lies where the field is particularly strong. Figure 3 shows Raman spectra of rhodamine bound on the surface of a 1 cm long slot waveguide having a total width of 850 nm and a void width of 150 nm. This spectrum is compared to the one obtained from rhodamine deposited on a calcium fluoride slide and measured using a Raman microscope in similar condition. In both cases, the monolayer is 7 ± 2 nm thick. For both curves, the photon background has not been subtracted and clearly shows the better SNR in the slot waveguide case. The difference in collection efficiency is enormous as obtaining a measurable spectrum with the confocal microscope required 40 times more power and 10 times longer acquisition time. This approach has recently allowed to measure the hybridization kinetics of DNA[15].

4. PLASMONIC ANTENNA ON WAVEGUIDE-BASED ON-CHIP RAMAN SPECTROSCOPY

Another approach to increase the SNR is to boost further the Raman signal without boosting the background from the silicon nitride material. This can be achieved using a plasmonic antenna such as a bow-tie antenna depicted in figure 4a. Indeed, such a structure creates a hot spot located between the 2 closest tips of the gold antenna (see figure 4b). A liquid analyte or a monolayer can easily fill the gap of the antenna and give rise to plasmonic enhanced Raman scattering (also known as surface enhanced Raman scattering). The plasmonic antenna is very small with typical dimensions on the order of tens of nm and similar gap size (see figure 4a), but the field enhancement is strong enough to make a Raman signal similar to propagation over several microns in a slot waveguide. To effectively be of any use for on-chip Raman spectroscopy, the antenna has to couple efficiently to a nanophotonic waveguide. The interface between the waveguide and the antenna can be realized simply by patterning the antenna on top of an existing nanophotonic waveguides [16, 17]. The antenna being a resonant structure, its design requires an optimization so that the field enhancement is strongest at the wavelength for which the Raman signal and the laser beam are expected [16]. In practice, we use antennas with the exact dimensions as depicted in figure 4a. Fabrication of both the antenna and the nanophotonic waveguide are performed via e-beam lithography.

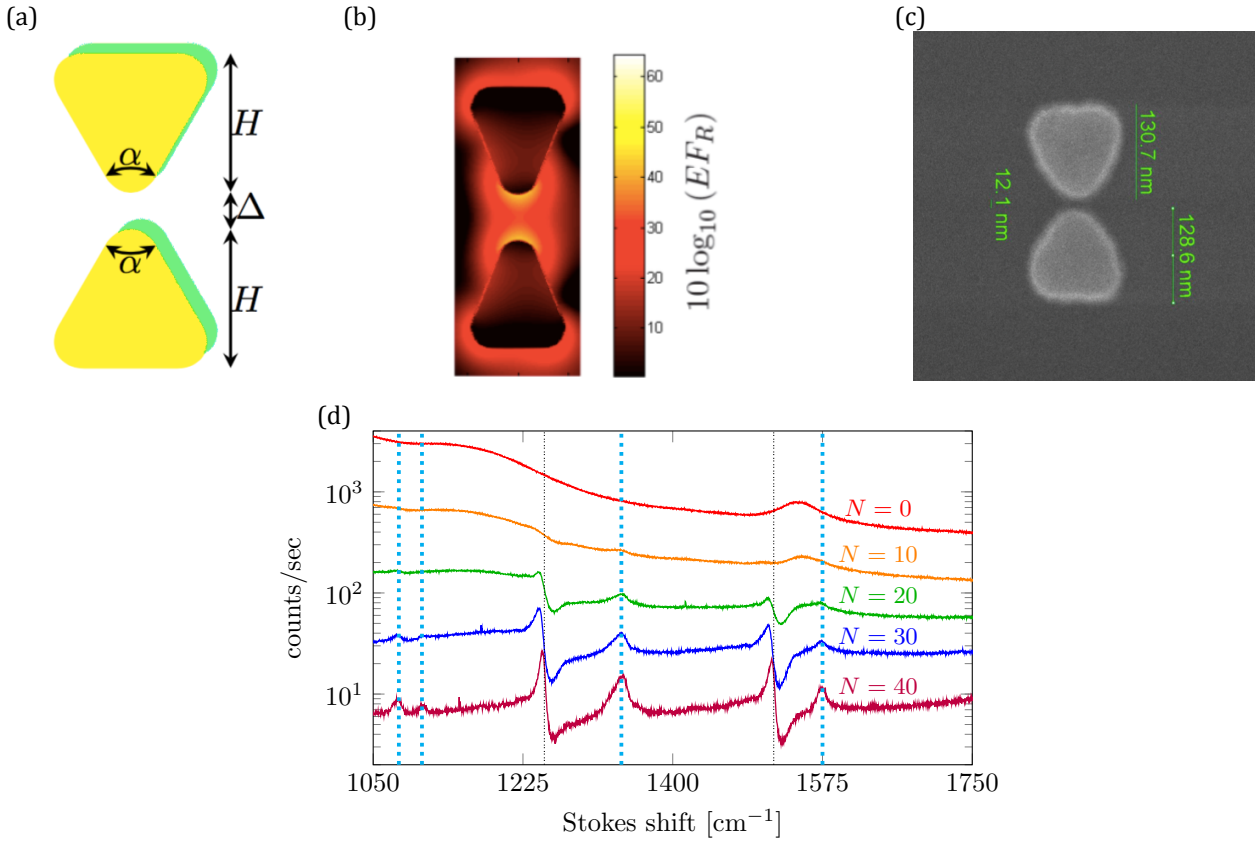

Fig 4. (a) Schematic of a bow-tie plasmonic antenna on top of a SiN photonic waveguide. The length H is 106±8nm, the gap Δ = 48±13 nm, the apex angle is α = 60° and the thickness is 30 nm. (b) Color plot of the field enhancement around the plasmonic antenna for excitation from the waveguide underneath. (c) SEM picture of a similar bow-tie antenna patterned via e-beam lithography. (d) Raman spectra obtained from ensembles of N antennas coated with NTP as the analyte under investigation.

Similarly, to the Raman conversion efficiency parameter η introduce at eq. 2 for waveguides, such a parameter can be introduced for a single antenna coupled to a waveguide:

$$\eta_a(\lambda_p,\lambda_s) = \frac{\rho\sigma(\lambda_s)}{2}\iiint \zeta(\mathbf{r},\lambda_p,\lambda_s)EF(\mathbf{r},\lambda_s)^2 EF(\mathbf{r},\lambda_p)^2 \mathrm{d}\mathbf{r} \qquad \text{(eq, 3)}$$

with $$\zeta(\mathbf{r},\lambda_p,\lambda_s) = \frac{n_g(\lambda_p)n_g(\lambda_s)\lambda_s^2|\mathbf{E}_{mode}(\mathbf{r},\lambda_p)|^2|\mathbf{E}_{mode}(\mathbf{r},\lambda_s)|^2}{n_{mode}\left(\iint \epsilon(\mathbf{r})|\mathbf{E}_{mode}(\mathbf{r},\lambda_s)|^2\mathrm{d}\mathbf{r}\right)\left(\iint \epsilon(\mathbf{r})|\mathbf{E}_{mode}(\mathbf{r},\lambda_p)|^2\mathrm{d}\mathbf{r}\right)}$$

In these equations, the factor *EF* is a field enhancement parameter defined as the ratio between the field strength in an unperturbed strip waveguide E_{mode}, and the field at the same position when an antenna is patterned on the waveguide $E_{antenna}$. This parameter requires 3-dimensional simulation of the whole structure and the reader can refer to [16,17] for more details.

To measure the actual response from a single antenna, the antenna has been coated with a monolayer of 4-nitrothiophenol (NTP). NTP is chosen because it binds selectively to gold but not to silicon nitride so that the evanescent field of the bare waveguide doesn't probe the analyte. Figure 4d presents the resulting Raman spectra acquired by *ensembles of antennas.* Indeed, a single antenna alone doesn't provide an identifiable Raman spectrum because the contribution from the bow-tie antenna is too weak in comparison to the background associated to the millimeters-long access waveguide. For as little as 10 antennas, the Raman spectrum is

measurable and especially the most prominent peak of NTP at 1340 cm^{-1} is clearly visible. For a larger number of antennas, we see an overall increase in signal to noise ratio, the appearance of extra peaks in the spectrum and a decrease of the signal. The decrease in signal is due to the particular measurement setup. The spectra are indeed taken in transmission so that light has to travel through all the antennas before reaching the spectrometer. By doing so, light experiences a strong absorption at each antenna so that overall the signal is reduced. In this configuration there is actually an optimal number of antenna for which the signal-to-noise ratio is maximal [17]. Extra peaks are related to the actual Raman spectrum of NTP (highlighted in shaded blue) but not only. The appearance of spurious peaks and a distortion of the broad background spectrum is due to the periodicity of the array of antennas. The antennas are indeed separated from each other by 10 μm so that this array acts as a higher order Bragg grating resulting in fringes in the overall transmission. This effect can easily be mitigated by putting the antennas much closer to each other and by randomizing their spacing. By accounting for the loss due to each antenna, it is possible to estimate η_A from the antenna ensemble spectra. The reconstructed value is $\eta_A = 2.6\ 10^{-15}$ and is in agreement with the expected $2.2\ 10^{-15}$ deduced from numerical simulation [16] of the structure and from knowledge of the Raman cross-section of NTP $\sigma = 3.58 \times 10^{-29}\ cm^2\ sr^{-1}$ for the resonance at 1340 cm^{-1}.

A direct comparison between the Raman spectrum obtained from a waveguide with the one obtained from an ensemble of antenna is a difficult task because the antennas are always on waveguides that can themselves collect a Raman signal even in the absence of an antenna. That is the reason why we have used two different monolayers for comparison plasmonic antenna to long SiN waveguides. NTP was used for antenna because it binds selectively to gold and rhodamine was used for SiN waveguides. Having compared experimental results and numerical simulations using equation eq. 1-3, we can proceed to a numerical comparison involving an identical analyte. Knowing the cross section of IPA ($\sigma = 7.9 \times 10^{-31}\ cm^2\ sr^{-1}$ for the peak at 819 cm^{-1}), we can estimate from simulation the conversion efficiency η_A that would be generated if the antenna where covered with IPA rather than being coated by a monolayer of NTP [18]. A comparison between this conversion efficiency and the one obtained using a strip waveguide indicates that a single antenna produces as much Raman signal as a 7 micrometer-long waveguide.

5. CONCLUSION AND FUTURE WORK

Nanophotonic waveguides provide a great way to enhance the Raman scattering from a liquid or a monolayer. The enhancement as compared to a Raman microscope is particularly impressive for single monolayers as conventional systems really struggle in these conditions. The major limitation of the strip and slot waveguide is the presence of a broadband background of photons generated by the SiN core of the waveguide. In contrast, plasmonic antennas allow confining the field entirely in the analyte so that they don't suffer from direct additional background. Unfortunately, the nitride waveguide that couples the light into and out of the antenna still creates a substantial background. The current SERS enhancement is still moderate in comparison to state of the art SERS substrates so that obtaining stronger Raman signals from a single antenna or an ensemble of tightly packed antennas seems feasible on the short term by improving their geometry. The great enhancement of the Raman signal implies a better tolerance to dark counts in the detector and ultimately the use of a uncooled CMOS sensor rather than a state of the art cooled CCD camera. Other solutions are being investigated to increase the SNR that involve using a material with lesser background or pushing the field outside of the waveguide using a non-resonant plasmonic waveguide. Various works[19, 21] are studying those possibilities.

6. REFERENCES AND AKNOWLEDGMENTS

The authors acknowledge imec, Leuven for fabrication of the waveguides, and the ERC Advanced Grant, Inspectra, Fonds Wetenschappelijk Onderzoek (FWO) and Bijzonder Onderzoeksfonds (BOF-UGent) for funding.

[1] Laserna, JJ, Modern techniques in Raman spectroscopy. New York, NY: John Wiley & Sons Ltd. (1996)
[2] Cheng, J.-X.. and Sunney Xie, X., Coherent Raman scattering microscopy, CRC press, (2016).
[3] Le Ru, E., and Etchegoin, P., Principles of Surface-Enhanced Raman Spectroscopy: and related plasmonic effects, Elsevier (2008).

[4] Li, J.; Chen, C.; Jans, H.; Xiumei, X.; Verellen, N.; Vos, I.; Okumura, Y.; Moshchalkov, V.V.; Lagae, L.; Van Dorpe, P., "300 mm Wafer-level, ultra-dense arrays of Au-capped nanopillars with sub-10 nm gaps as reliable SERS substrates", Nanoscale 6, 12391– 12396 (2014)
[5] Benabid, F, Knight, J.C., Antonopoulos, G., and Russell, P. St J., "Stimulated Raman scattering in hydrogen-filled hollow-core photonic crystal fiber", Science 298 (5592), 399-402 (2002)
[6] Kanger JS, Otto C, Slotboom M, Greve J., "Waveguide Raman spectroscopy of thin polymer layers and monolayers of biomolecules using high refractive index waveguides", J. Phys. Chem. 100, 3288 – 3292 (1996)
[7] Marquardt, B.J., Vahey, P.G., Synovec, R.E. and Burgess, L.W., "A Raman waveguide detector for liquid chromatography", Analytical chemistry, 71(21), 4808-4814. (1999)
[8] Rabolt JF, Santo R, Swalen JD., "Raman measurements on thin polymer films and organic monolayers", Appl. Spectrosc. 34, 517 – 521 (1980)
[9] Bradshaw JT, Mendes SB, Saavedra SS., "Planar integrated optical waveguide spectroscopy", Anal. Chem. 77, 28A – 36A. (2005)
[10] Dhakal, A., Subramanian, A.Z., Wuytens, P., Peyskens, F., Le Thomas, N. and Baets, R., "Evanescent excitation and collection of spontaneous Raman spectra using silicon nitride nanophotonic waveguides", Opt. Lett. 39 (13), 4025 (2014)
[11] Nie, X, Ryckeboer, E.M.P., Roelkens, G., and Baets, R., "Novel Concept for a Broadband Co-propagative Stationary Fourier Transform Spectrometer Integrated on a Si3N4 Waveguide Platform", Conference on Lasers and Electro-Optics (CLEO) 2016, United States, (2016)
[12] Bogaerts, W., Dumon, P., Van Thourhout, D., Taillaert, D., Jaenen, P, Wouters, J, Beckx, S, Baets, S, "Compact Wavelength-Selective Functions in Silicon-on-Insulator Photonic Wires", J. Selected Topics in Quantum Electronics, 12(6), 1394-1401 (2006)
[13] Subramanian, A., Neutens, P, Dhakal, A, Jansen, R, Claes, T, Rottenberg, X, Peyskens, F, Selvaraja, S, Helin, P, Du Bois, B, Leyssens, K, Severi, S, Deshpande, P, Baets, R, Van Dorpe, P, "Low-loss singlemode PECVD silicon nitride photonic wire waveguides for 532-900 nm wavelength window fabricated within a CMOS pilot line", IEEE Photonics Journal, 5(6), 2202809 (2013)
[14] Dhakal, A, Raza, A, Peyskens, F, Subramanian, A, Clemmen, S, Le Thomas, N, Baets, R, "Efficiency of evanescent excitation and collection of spontaneous Raman scattering near high index contrast channel waveguides", Optics express, 23(21), 27391-27404 (2015)
[15] Dhakal, A., Wuytens, P.C., Peyskens, F., Jans, K., Thomas, N.L. and Baets, R., "Nanophotonic waveguide enhanced Raman spectroscopy of biological submonolayers," ACS Photonics 3(11) , 2141-2149 (2016).
[16] Peyskens, F., Subramanian, A., Neutens, P., Dhakal, A., Van Dorpe, P., Le Thomas, N., Baets, R., "Bright and dark plasmon resonances of nanoplasmonic antennas evanescently coupled with a silicon nitride waveguide", Optics Express, 23(3), 3088-3101 (2015)
[17] Peyskens, F., Dhakal, A., Van Dorpe, P., Le Thomas, N., Baets, N., "Surface Enhanced Raman Spectroscopy Using a Single Mode Nanophotonic-Plasmonic Platform", ACS Photonics, 3(1), 102-108 (2016).
[18] Dhakal, A., Peyskens, F., Clemmen, S., Raza, A., Wuytens, P.C. , Zhao, H., Le Thomas, N., Baets, R., "Single mode waveguide platform for spontaneous and surface-enhanced on-chip Raman spectroscopy", Interface Focus 6(4) 20160015 (2016)
[19] Evans, C.C., Liu, C. and Suntivich, J., "TiO2 Nanophotonic Sensors for Efficient Integrated Evanescent Raman Spectroscopy",ACS Photonics,3(9), 1662 (2016).
[20] Tang, F., Adam, PM, and Boutami, S, "Theoretical investigation of SERS nanosensors based on hybrid waveguides made of metallic slots and dielectric strips." Optics Express 24 (19), 21244 (2016)
[21] Wang, Z., Zervas, M.N., Bartlett, P.N. and Wilkinson, J.S., "Surface and waveguide collection of Raman emission in waveguide-enhanced Raman spectroscopy", Optics Letters, 41(17), 4146-4149 (2016)